

Analysis of Material Flow and Phase Transformation in Friction Hydro-Pillar Processing of 1045 Steel

Moosa Sajed

Department of Mechanical Engineering,
University of Birjand, Iran
E-mail: m.sajed@birjand.ac.ir

Seyed Mohammad Hossein Seyedkashi*

Department of Mechanical Engineering,
University of Birjand, Iran
E-mail: seyedkashi@birjand.ac.ir

*Corresponding author

Received: 18 May 2020, Revised: 22 June 2020, Accepted: 22 July 2020

Abstract: In the present study, a 3D finite element model was developed using DEFORM commercial software to analyse the material flow and phase transformation, as two key phenomena affecting the joint properties in friction hydro-pillar processing of 1045 steel alloy. The microstructure changes significantly due to the high temperature and strain rate. The final microstructure was intergranular pearlite and grain boundary allotriomorphic ferrite. Pearlite was the dominant phase at the final microstructure; thus, its volume fraction was used to validate the model where a good agreement was obtained with the experiment. According to the model, the pearlite volume fraction varies from 100% to 70% moving from the bottom of the stud to the top. The model suggests an inverse relation between the strain rate and pearlite volume fraction. The highest temperature which was experienced in the welding step was 1490 °C while it dropped to 890 °C in the forging step. Downward and then radial material flow was detected in the welding step while upward extrusion of material was the dominant material flow pattern during the forging step. Flash was formed mainly in the forging step from stud side material.

Keywords: Friction Hydro-Pillar Processing, Material Flow, 1045 Steel, Solid-State Processing, Phase Transformation

Reference: Moosa Sajed, Seyed Mohammad Hossein Seyedkashi, “Analysis of Material Flow and Phase Transformation in Friction Hydro-Pillar Processing of 1045 Steel”, Int J of Advanced Design and Manufacturing Technology, Vol. 13/No. 4, 2020, pp. 31–37. DOI: 10.30495/admt.2020.1900258.1198

Biographical notes: **Moosa Sajed** is a PhD candidate in Mechanical Engineering at the University of Birjand. His current research interest is solid-state welding mainly friction-based welding process. He also works on developing finite element models for processes where severe plastic deformation takes place. He received his M.Sc. in Mechanical Engineering from Iran University of Science and Technology (2011). **Seyed Mohammad Hossein Seyedkashi** received his PhD in Mechanical Engineering from Tarbiat Modares University, Tehran, Iran (2012). He is now an associate professor at Department of Mechanical Engineering, University of Birjand, Birjand, Iran. His research interests are metal forming, friction welding, and optimization methods.

1 INTRODUCTION

Friction based solid-state processes are used in various industries and are interested by researchers due to their simplicity, applicability, and unique features [1]. Friction stir welding is the most popular friction-based welding process for aluminium alloys [2]. However, Friction Hydro Pillar Processing (FHPP) is a solid-state process which is mainly developed to repair cracks in steel alloys. In FHPP, a rotary stud rotates into a blind groove which is then filled with plasticized material of the stud. A final forging is required after the filling to improve filled material [3]. It is a creative method to repair cracks which occurs in depth of thick steel plates in components which are in service and could not be repaired by conventional fusion methods. As a solid-state process, material flow is important and affects the processed sample in all aspects. Microstructure changes during the process also dominate mechanical properties of the joint. There are issues regarding experimental evaluation of these phenomena. Thus, it is necessary to develop a model which is able to predict both material flow and microstructure changes during friction hydro-pillar processing.

Friction hydro-pillar processing and friction taper welding, as a variant of the main process, are investigated by many researchers. Cui et al. [3] investigated friction taper plug welding of low alloy structural steel. They investigated the process conditions, affecting parameters, and welding defects. Buzzatti et al. [4] studied the toughness of the friction hydro-pillar processed offshore mooring chain steel with three different axial forces and reported enhanced toughness increasing the axial force. Vicharapu et al. [5] also studied friction hydro-pillar processing. Meinhardt et al. [6] investigated friction hydro-pillar processing of duplex stainless steels. Hattingh et al. [7] studied the effect of process parameters on friction taper stud welding of AISI 4140 steel alloy. Kanan et al. [8] studied friction hydro-pillar processing of high carbon steel, while Chludzinski et al. [9] investigated C-Mn steel. Yin et al. [10] tried underwater friction taper plug welding of pipeline steel. Xu et al. [11] reported that a rounded corner should be used at the bottom of the bore to achieve the best filling process. They reported that more defects occur at the bottom of the bore. Some numerical investigations were also carried out. Li et al. [12] investigated friction hydro-pillar processing of Q345 steel numerically. They used the temperature field to validate the simulation. They investigated the plastic metal layer, frictional interface (FI), temperature field, and microstructure. Landell et al. [13] investigated the material flow during friction hydro-pillar processing. They reported that the centre of the stud deforms in shear planes. The outer surface of stud also forms the unbounded flash. It is important to achieve joints with

desired characteristics. Sajed [14] introduced a two-stage process to refill the keyhole in friction stir spot welding that is then used to achieve stronger joints in friction stir spot welding of polyethylene sheets using SiC powder as a reinforcement [15]. Similar reinforcement was carried out in friction hydro-pillar processing of St37 steel [16]. They placed SiC powder in the centre of the stud that then was distributed in the welding zone.

Although there are many investigations on friction hydro-pillar processing, there is a very limited number of investigations concerning the simulation of the process. On the other hand, 2D models were developed in the present literature that are valuable, but could not completely describe 3D material flow during the process. The phase transformation also was not considered in the reports that are available in the literature. As mentioned before, material flow and phase transformation determine the joint characteristics. Therefore, there is a need to develop a model that is capable of predicting the phase transformation and material flow. In the present paper, a 3D finite element was developed using commercial DEFORM software to predict material flow and phase transformation in friction hydro-pillar processing of 1045 steel alloy. The pearlite phase volume fraction was used to validate the model. The results of the simulation were in good agreement with the experiment.

2 EXPERIMENT

To validate the numerical model, an experiment was also conducted. St37 mild steel plate with a thickness of 25 mm was used as a base plate. A bore with a diameter of 16 mm and a depth of 20 mm was drilled. The stud material was 1045 steel alloy. It was machined with a diameter of 15.5 mm and a length of 90 mm. A shank was also considered with a diameter of 18 mm to be used as a fastening part of the stud. The stud, base plate, and welded sample are presented in "Fig. 1".

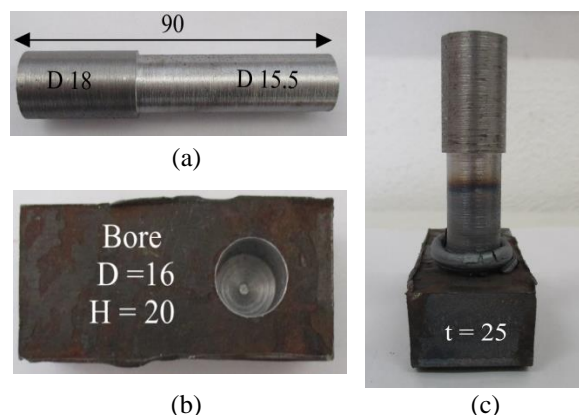


Fig. 1 (a): Stud, (b): bore, and (c): the welded sample.

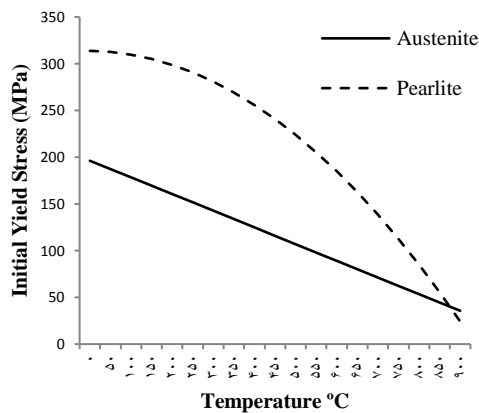
The chemical composition of St37 and 1045 steel alloys are tabulated in “Table 1 and Table 2”, respectively. The experiment was carried out with a rotational speed of 3000 rpm, an axial force of 20 kN, a forging force of 25 kN, and a burn-off of 14 mm.

Table 1 Chemical composition of St37 (wt. %) [17]

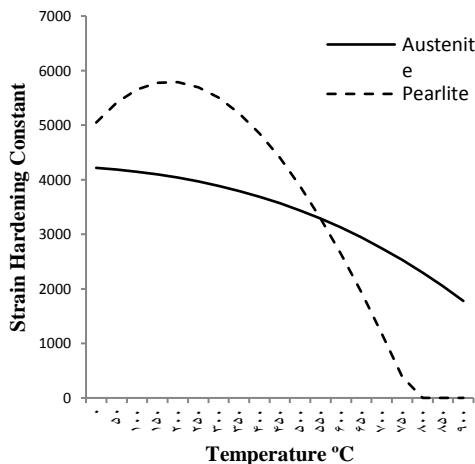
C	Si	Mn	P
0.11	0.03	0.56	0.007
S	Cr	Ni	Fe
0.005	0.07	0.03	Bal.

Table 2 Chemical composition of 1045 steel (wt. %) [11]

C	Si	Mn	P
0.467	0.257	0.750	0.011
S	Cr	Ni	Mo
0.008	0.017	0.013	0.002
Al	Cu	Pb	Fe
0.048	0.005	0.002	Bal.



(a)



(b)

Fig. 2 Coefficients of the material model, (a) Y vs. temperature, and (b) H vs. temperature [18].

3 NUMERICAL MODEL

The linear hardening model was used as material model which can be illustrated with the Eq. (1) [18]:

$$\sigma = Y(T, A) + H(T, A)\epsilon \tag{1}$$

Where, σ is the flow stress, Y is the initial yield stress which is a function of temperature (T) and atom content (A), H is the strain hardening constant which is also a function of temperature and atom content, and ϵ is the effective plastic strain. Y and H are temperature-dependent variables which are depicted in “Fig. 2” for austenite and pearlite.

The yield function type and the hardening rule were von-Mises and isotropic, respectively, for both austenite and pearlite. Young's modulus was temperature-dependent (“Fig. 3”).

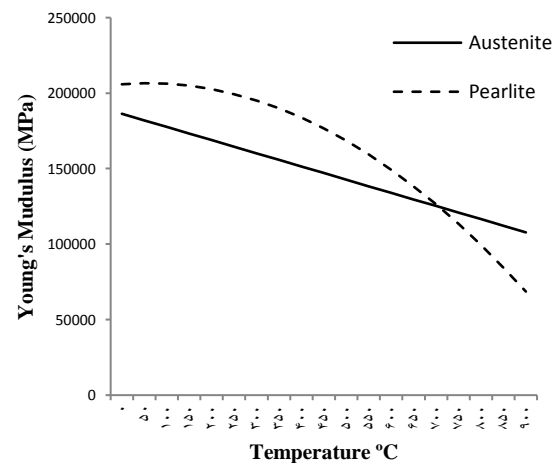


Fig. 3 Young's modulus vs. temperature [18].

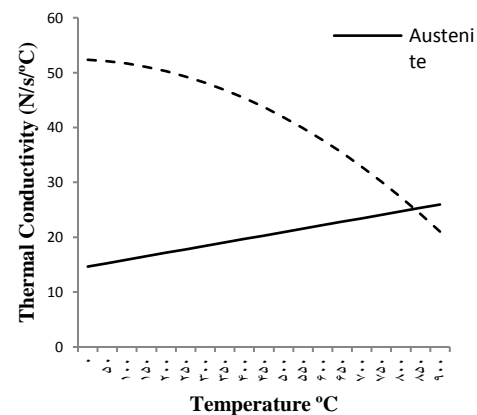


Fig. 4 Thermal conductivity vs. temperature [18].

The Poisson's ratio was constant at 0.3 for all phases. The thermal expansion coefficients were 2×10^{-5} and 1.5×10^{-5} $1/^\circ\text{C}$ for austenite and pearlite, respectively. The thermal conductivity was also temperature-dependent which is depicted in "Fig. 4". The heat capacity of austenite was $4.631 \text{ N/mm}^2/\text{s}$ while it was temperature-dependent for pearlite according to "Fig. 5". The density, hardness, and diffusion coefficients were for all phases were 7.85 g/cm^3 , 55 HRC, and $7.4 \times 10^{-5} \text{ mm}^2/\text{s}$, respectively.

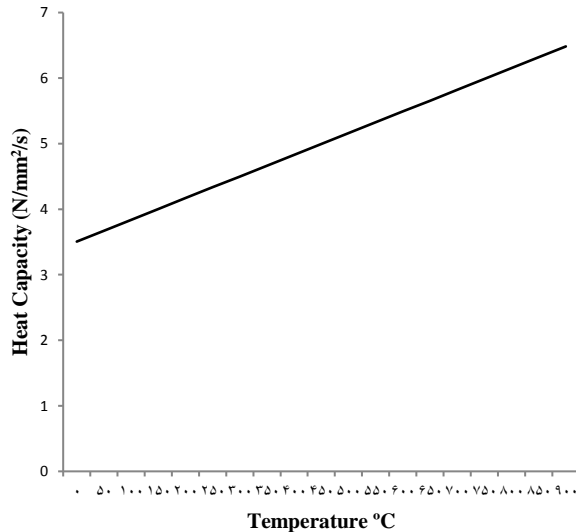


Fig. 5 Heat capacity vs. temperature for pearlite [18].

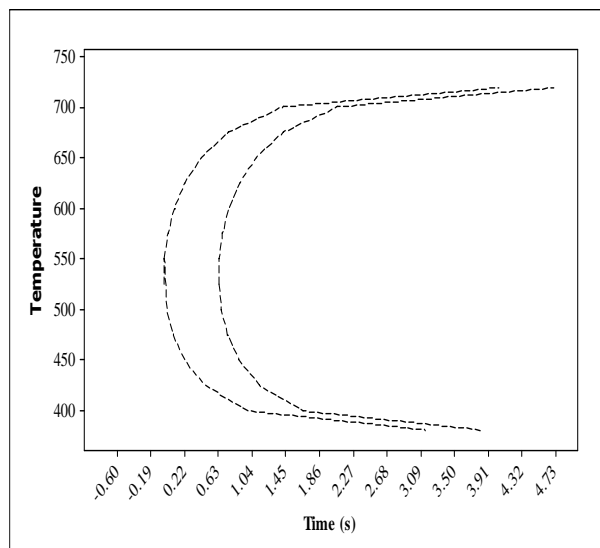


Fig. 6 TTT diagram of 1045 steel [18].

There are several models to simulate the kinetics of phase transformation. In the present paper, the simplified diffusion model was used to simulate the pearlite-austenite transformation as follows [18]:

$$\zeta_J = 1 - \exp \left\{ A \left(\frac{T_{el} - T_s}{T_e - T_s} \right)^D \right\} \quad (2)$$

Where, ζ_J is the volume fraction transformed, T_{el} is the average element temperature in $^\circ\text{C}$, T_s is the starting temperature of the transformation in $^\circ\text{C}$, T_e is the ending temperature of the transformation in $^\circ\text{C}$, A is a constant, and D is also a constant. In the present study, the values of A , D , T_s , and T_e were -4, 2, $722 \text{ }^\circ\text{C}$, and $816 \text{ }^\circ\text{C}$, respectively. For the transformation of austenite to pearlite, the TTT curve was used as illustrated in "Fig. 6".

Figure 7 presents the finite element model. The Lagrangian incremental method together with the direct iteration method were used. The process conditions were the same as the experiment. 3D tetrahedral meshes with a number of 32000 was used for meshing both stud and bore. Remeshing was also used whenever the shape of elements was distorted in a way that the solution was not converged. All contact surfaces were considered to be separable. For all contact surfaces, friction was considered to be shear-type with a constant coefficient of 0.7 and the heat transfer coefficient was $5 \text{ N/s/mm}^\circ\text{C}$.

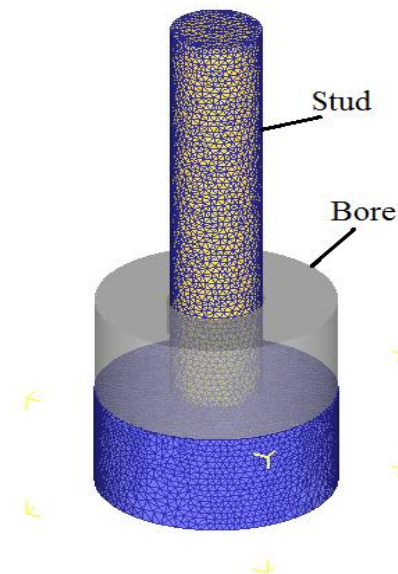


Fig. 7 The finite element model.

4 RESULTS & DISCUSSION

Due to high temperature and strain rate that are experienced by the workpiece during the process, considerable changes take place in its microstructure that significantly affects the mechanical properties of the

welded sample. In fact, the mechanical properties of the joint are affected by both material flow and microstructure changes.

Figure 8 presents material flow at the cross-section of the processed sample during the process. Figure 8(a) presents the cross-section before contact. When the welding starts, the dominant material flow directions are downward and sideward as shown in “Fig. 8(b)”. Downward material flow is governed by the pressing of the stud against the bottom of the bore where the outer surface of the stud flows to fill the gap between the stud and the bore wall. It is evident that the central material mainly moves toward the bottom of the bore and there is no considerable sideward movement. This indicates that filling of the gap is fulfilled by side material where excess material moves upward and makes the flash. The forging step is presented in “Fig. 8(c)”. In this step, there is a significant downward movement and the flash becomes bigger due to the upward material extrusion at the bore edge.

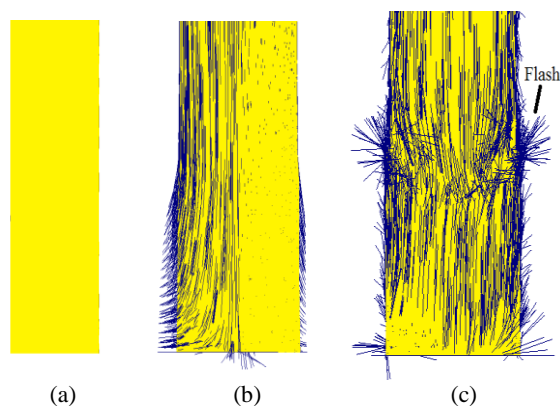


Fig. 8 Material flow during the process: (a): Before contact, (b): welding step, and (c): forging step.

Figure 9 presents the microstructure of the as-received and welded sample. The microstructure of as-received material contains ferrite (light area) and pearlite (dark zones). The microstructure of the processed sample contains overheated structures. The final microstructure contains intergranular pearlite, grain boundary allotriomorphic ferrite (BAF), and secondary Widmanstätten ferrite (SWF). In this process, austenite grains were transformed into pearlite while ferrite was formed from the grain boundaries. The image processing technique was applied to evaluate the percentage of pearlite in each image.

The volume fraction of pearlite on the cross-section of the processed zone at the end of welding and forging steps are presented in “Fig. 10(a) and (b)”, respectively. In the welding step, there is almost no pearlite at the end of the stud, while the volume fraction of pearlite increases by moving from the bottom to the top of the processed zone.

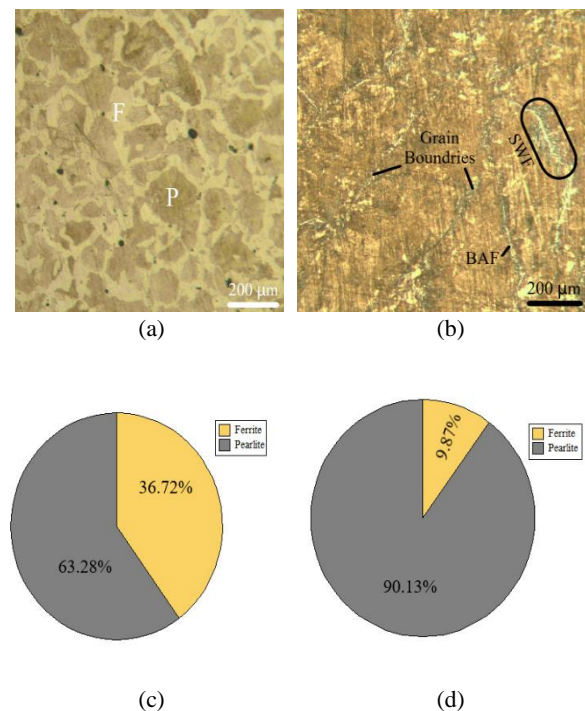


Fig. 9 Microstructure of: (a): as-received 1045 steel, and (b): the processed material. Phase fraction analysis of (c): the as-received material and (d) the processed material.

The pearlite volume fraction percentage varies from 1.8% to 81.5% in this step. However, in the forging step, more pearlite is formed and the pearlite volume fraction varies from 69.9% to 98% in the processed zone. Figures 9(c) and (d) present results of volume fraction for as-received and processed materials, respectively. The pearlite percentage was increased from 63.28% to 90.13% by the process. The pearlite percentage of the processed specimen is in a good agreement with the results of the simulation.

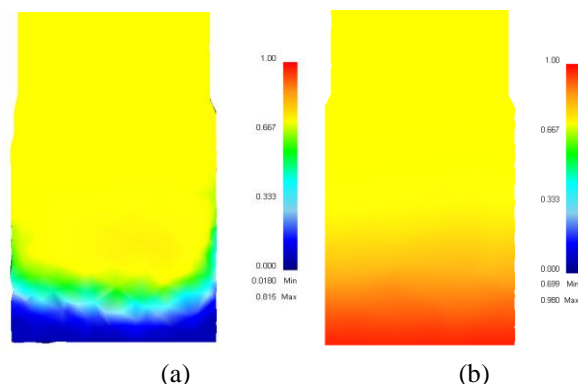


Fig. 10 The pearlite volume fraction in: (a): the welding step, and (b): the forging step.

Pearlite consists of ferrite and cementite in a lamellar structure. Therefore, time is needed for carbide and pearlite formation by diffusion. In the forging step, this time is supplied for the specimen. On the other hand, a

high strain rate makes conditions difficult for diffusion. In the forging step, the stud experiences much lower strain rate, and more pearlite could be transformed. In the welding stage, the strain rate is also important. The strain rate is highest at the bottom of the stud while it decreases moving from bottom to top; see “Fig. 11(a)”. The pearlite percentage also follows the same pattern. In the forging step, the same relationship could be identified between strain rate and pearlite formation comparing “Fig. 10(b) and Fig. 11(b)”. On the other hand, due to the short time of the process, it seems that the strain rate is the dominant parameter affecting the phase transformation during the process.

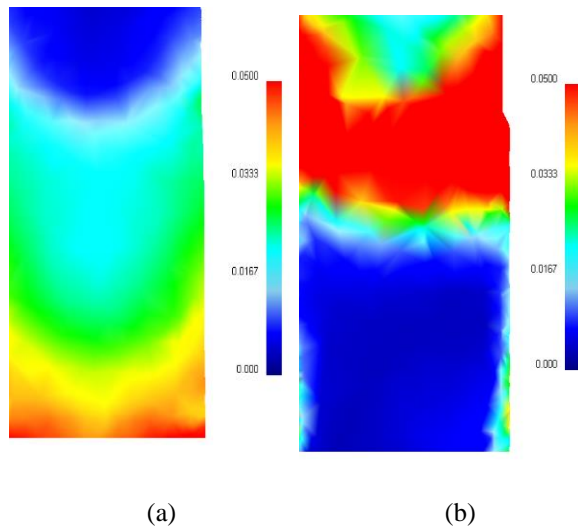


Fig. 11 Effective strain-rate in: (a): welding, and (b): forging steps.

Temperature is an important parameter that affects joint formation, microstructure evolution, and mechanical properties as a result. Friction hydro-pillar processing is considered as a solid-state process; however, the temperature rises considerably during the process. Several zones in the processing area experience even near liquidus point temperature locally. Figure 12(a) presents the temperature range that is experienced by the material during the welding step. The maximum temperature is 1490 °C that is experienced at the bottom of the stud. Moving from bottom to top, the temperature drops dramatically so that it becomes 600 °C at the top of the processed zone. The maximum temperature is experienced at the bottom of the stud because the highest frictional force is located there. During the process, a downward force is exerted to the stud that presses the stud to the bore bottom and because the highest normal force is at the bottom, the frictional force also is the highest, and the heat generation and temperature rise are the highest as well. Due to the heat conductivity of the processed alloys, the temperature drops dramatically when the spinning of the stud is stopped, i.e. in the

forging step. In this step, the highest temperature is around 900 °C. Again, the highest temperature is experienced at the bottom of the stud as seen in “Fig. 12(b)”.

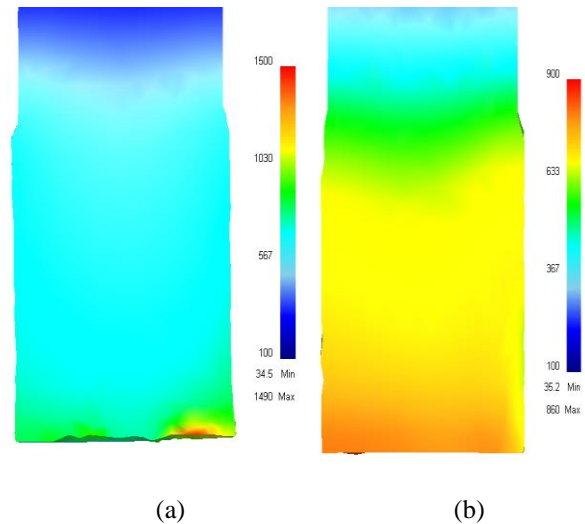


Fig. 12 Temperature distribution in (a) welding and (b) forging steps.

5 CONCLUSION

In the present study, a 3D finite element model was developed to analyse the material flow and phase transformation during friction hydro-pillar processing of 1045 steel alloy. Pearlite volume fraction was used to validate the model. Main results of the present study are as follows:

- Due to the high temperature and strain rate, a significant change occurs in the microstructure. The final microstructure contains intergranular pearlite and grain boundary allotriomorphic ferrite.
- Pearlite is the dominant phase at the final microstructure of the processed zone. The volume fraction of the pearlite decreases from the bottom of the stud to the top.
- Strain rate is the dominant parameter affecting the phase transformation.
- The highest temperature in the welding and forging steps are 1490 °C and 890 °C, respectively.
- The material flow pattern is downward and then radial in the welding step. Flash is formed mainly in the forging step and contains stud side material.

6 NOMENCLATURE

Symbol	Description	Unit
σ	Effective flow stress	MPa

ε	Effective plastic strain	-
Y	Initial yield stress	MPa
T	Temperature	°C
A	Atom content	-
H	Strain hardening constant	-
ζ_j	Volume fraction transformed	-
T_{el}	Average element temperature	°C
T_s	Starting temperature of the transformation	°C
T_e	Ending temperature of the transformation	°C

REFERENCES

- [1] Sattari, S., Bisadi, H., and Sajed., M., Mechanical Properties and Temperature Distributions of Thin Friction Stir Welded Sheets of AA5083, *International Journal of Mechanics and Applications*, Vol. 2, No. 1, 2012, pp. 1-6, DOI. 10.5923/j.mechanics.20120201.01
- [2] Sajed, M., Bisadi, H., Experimental Failure Study of Friction Stir Spot Welded Similar and Dissimilar Aluminum Alloys, *Welding in the World*, Vol. 60, No. 1, 2016, pp. 33-40, DOI. 10.1007/s40194-015-0268-6.
- [3] Cui, L., Yang, X., Wang, D., Cao, J., and Xu, W., Experimental Study of Friction Taper Plug Welding for Low Alloy Structure Steel: Welding Process, Defects, Microstructures, and Mechanical Properties, *Materials & Design*, Vol. 62, 2014, pp. 271-281, DOI. 10.1016/j.matdes.2014.05.026.
- [4] Buzzatti, D. T., Chludzinski, M., Santos, R. E., Buzzatti, J. T., Lemos, G. V. B., Mattei, F., Marinho, R. R., Paes, M. T. P., and Reguly, A., Toughness Properties of a Friction Hydro Pillar Processed Offshore Mooring Chain Steel, *Journal of Materials Research and Technology*, Vol. 8, No. 3, 2019, pp. 2625-2637, DOI. 10.1016/j.jmrt.2019.04.002.
- [5] Vicharapu, B., Kanan, L. F., Clarke, T., and De, A., An Investigation On Friction Hydro-Pillar Processing, *Science and Technology of Welding and Joining* Vol. 22, No. 7, 2017, pp. 555-561, DOI. 10.1080/13621718.2016.1274849.
- [6] Meinhardt, C. P., Chludzinski, M., Ribeiro, R. F., Rocha, C. L. F., Santos, A. C. S., and Strohaecker, T. R., Evaluation of Friction Hydro-Pillar Processing Welding in Duplex Stainless Steels (UNS S31803), *Journal of Materials Processing Technology*, Vol. 246, 2017, pp. 158-166, DOI. 10.1016/j.jmatprotec.2017.03.010.
- [7] Hattingh, D. G., Bulbring, D. L. H., Els-Botes, A., and James, M. N., Process Parameter Influence On Performance of Friction Taper Stud Welds in AISI 4140 steel, *Materials & Design*, Vol. 32, No. 6, 2011, pp. 3421-3430, DOI. 10.1016/j.matdes.2011.02.001.
- [8] Kanan, L. F., Vicharapu, B., Bueno, A. F. B., Clarke, T., and De, A., Friction Hydro-Pillar Processing of a High Carbon Steel: Joint Structure and Properties, *Metallurgical and Materials Transactions B*, Vol. 49, No. 2, 2018, pp. 699-708, DOI. 10.1007/s11663-018-1171-5.
- [9] Chludzinski, M., Paes, M. P., Bastian, F. L., and Strohaecker, T. R., Fracture Toughness of Friction Hydro-Pillar Processing Welding in C-Mn Steel, *Materials & Design*, Vol. 33, 2012, pp. 340-344, DOI. 10.1016/j.matdes.2011.07.056.
- [10] Yin, Y., Yang, X., Cui, L., Wang, F., and Li, S., Material Flow Influence On the Weld Formation and Mechanical Performance in Underwater Friction Taper Plug Welds for Pipeline Steel, *Materials & Design*, Vol. 88, 2015, pp. 990-998, DOI. 10.1016/j.matdes.2015.09.123.
- [11] Xu, Y. C., Jing, H. Y., Han, Y. D., and Xu, L. Y., Numerical Simulation of the Effects of Various Stud and Hole Configurations On Friction Hydro-Pillar Processing, *International Journal of Mechanical Sciences*, Vol. 90, 2015, pp. 44-52, DOI. 10.1016/j.ijmecsci.2014.10.025.
- [12] Li, W., Jiang, D., Yang, L., Pan, J., Qu, R., and Sun, T., Numerical Simulation of Temperature Field and Prediction of Microstructure in Friction Hydro Pillar Processing, *Journal of Materials Processing Technology*, Vol. 252, 2018, pp. 370-380, DOI. 10.1016/j.jmatprotec.2017.10.001.
- [13] Landell, R., Kanan, L. F., Buzzatti, D., Vicharapu, B., De A., and Clarke, T., Material Flow During Friction Hydro-Pillar Processing, *Science and Technology of Welding and Joining*, Vol. 25, No. 3, 2020, pp. 228-234, DOI. 10.1080/13621718.2019.1679963.
- [14] Sajed, M., Parametric Study of Two-Stage Refilled Friction Stir Spot Welding, *Journal of Manufacturing Processes*, Vol. 24, 2016, pp. 307-317, DOI. 10.1016/j.jmapro.2016.09.011.
- [15] Sajed, M., Seyedkashi, S. M. H., A Novel Technique for Keyhole-Less Reinforced Friction Stir Spot Welding of Polyethylene Sheets, *International Journal of Advanced Design and Manufacturing Technology*, Vol. 12, No. 4, 2019, pp. 47-56.
- [16] Sajed, M., Seyedkashi, S. M., Solid-State Micro-Alloying of Thick st37 Steel Plates with Sic Powder Using a Modified Friction Hydro-Pillar Process, *Journal of Materials Research and Technology*, Vol. 9, No. 4, 2020, pp. 7158-7171, DOI. 10.1016/j.jmrt.2020.04.068.
- [17] Jafarzadegan, M., Feng, A. H., Abdollah-Zadeh, A., Saeid, T., Shen, J., and Assadi, H., Microstructural Characterization in Dissimilar Friction Stir Welding Between 304 Stainless Steel and st37 Steel, *Materials Characterization*, Vol. 74, 2012, pp. 28-41, DOI. 10.1016/j.matchar.2012.09.004.
- [18] DEFORM, SFTC. "V11. 0 (PC) Documentation."